Advanced Fiber Materials (2023) 5:1008–1024
https://doi.org/10.1007/s42765-023-00266-8

RESEARCH ARTICLE

Elastic Fiber-Reinforced Silk Fibroin Scaffold with A Double-Crosslinking Network for Human Ear-Shaped Cartilage Regeneration

Qianyi Wang[1,2] · Xinyue Ran[1,2] · Jian Wang[1] · Sinan Wang[1,2] · Peiling Zhang[1] · Erji Gao[1] · Baoshuai Bai[1] · Junfeng Zhang[1,3] · Guangdong Zhou[1,2] · Dong Lei[1,3]

Received: 8 November 2022 / Accepted: 30 January 2023 / Published online: 20 February 2023

Abstract

Tissue engineering provides a promising approach for regenerative medicine. The ideal engineered tissue should have the desired structure and functional properties suitable for uniform cell distribution and stable shape fidelity in the full period of in vitro culture and in vivo implantation. However, due to insufficient cell infiltration and inadequate mechanical properties, engineered tissue made from porous scaffolds may have an inconsistent cellular composition and a poor shape retainability, which seriously hinders their further clinical application. In this study, silk fibroin was integrated with silk short fibers with a physical and chemical double-crosslinking network to fabricate fiber-reinforced silk fibroin super elastic absorbent sponges (Fr-SF-SEAs). The Fr-SF-SEAs exhibited the desirable synergistic properties of a honeycomb structure, hygroscopicity and elasticity, which allowed them to undergo an unconventional cyclic compression inoculation method to significantly promote cell diffusion and achieve a uniform cell distribution at a high-density. Furthermore, the regenerated cartilage of the Fr-SF-SEAs scaffold withstood a dynamic pressure environment after subcutaneous implantation and maintained its precise original structure, ultimately achieving human-scale ear-shaped cartilage regeneration. Importantly, the SF-SEAs preparation showed valuable universality in combining chemicals with other bioactive materials or drugs with reactive groups to construct microenvironment bionic scaffolds. The established novel cell inoculation method is highly versatile and can be readily applied to various cells. Based on the design concept of dual-network Fr-SF-SEAs scaffolds, homogenous and mature cartilage was successfully regenerated with precise and complicated shapes, which hopefully provides a platform strategy for tissue engineering for various cartilage defect repairs.

Keywords Silk fibroin · Fiber-reinforced · Elastic scaffold · Cellular distribution · Cartilage regeneration

Introduction

The development of tissue engineering is gradually changing traditional medical therapy and further evolving into regenerative medicine for clinical application [1, 2]. Biomaterial scaffolds are a vital component in the field of tissue

Qianyi Wang, Xinyue Ran and Jian Wang have contributed equally to the work.

✉ Junfeng Zhang
jfzhang_dr@163.com

✉ Guangdong Zhou
guangdongzhou@126.com

✉ Dong Lei
leidongjesse@qq.com

[1] Department of Plastic and Reconstructive Surgery, Shanghai 9th People's Hospital, Shanghai Jiao Tong University School of Medicine, Shanghai Key Lab of Tissue Engineering, Shanghai 200011, People's Republic of China

[2] Research Institute of Plastic Surgery, Weifang Medical University, Weifang 261053, People's Republic of China

[3] Department of Cardiology, Shanghai 9th People's Hospital, Shanghai Jiao Tong University School of Medicine, Shanghai 200011, People's Republic of China

engineering, as they provide a suitable mechanical strength, space and environment for cell adhesion, growth and development [3, 4]. The ideal cell scaffold, however, should not only provide space for growth and temporary support but also have a good affinity, be efficient in integrating cells with themselves and maintain a stable shape long-term to meet the practical needs of tissue defects and repair in clinical applications [5, 6].

Many studies have attempted to solve the challenge of constructing scaffolds with a high-density inoculation and uniform distribution of seed cells [7–9]. Porous scaffolds have been widely used in tissue regeneration. Stable porous structures can provide a matrix surface for cell adhesive growth and facilitate nutrient penetration for cell activity [10]. However, porous scaffolds have been mostly inoculated by drip injection, in which the distribution of cells within scaffolds relies on gravity and hydrophilicity. This uncontrolled cell inoculation model causes most of the cells to adhere to the outer surface of the scaffold, while the distribution of cells inside the scaffold is limited. Therefore, some attempts have been made to increase the pore size of the scaffold to improve the uniformity of inoculation, but this can also lead to excessive cell loss and low inoculation efficiency [11, 12].

Another key factor of tissue regeneration is maintaining the precise three-dimensional shape of scaffolds in the full period of in vitro culture and in vivo implantation [13, 14]. The shape of regenerated tissue should match the shape of the tissue defect of the patient, which is essential for the clinical translation of tissue engineering [15]. Synthetic polymer biomaterials can have effectively controlled mechanical properties, but their biological activity is limited. Natural materials have better activity, but porous scaffolds made from natural materials have difficulty maintaining their original morphology and microstructure in the application process due to their weak mechanical characteristics and high porosity. Silk cellulose has reportedly been approved by the FDA as a biodegradable natural protein material and is widely used for cardiovascular and skin regeneration as well as soft tissue regeneration due to its superior cellular affinity [16–18]. Silk fibroin scaffolds are formed mainly by the weak interactions of the molecular chain β-sheets and crystallization [19]. However, the low modulus and mechanical strength of silk fibroin porous scaffolds make it difficult for them to resist the dynamic mechanical environment in vivo and maintain the designed structure of regenerated tissue [20, 21]. This limitation has greatly hindered the clinical application of silk proteins, and previously reported porous scaffolds designed using silk proteins have not yet been able to meet this need.

Fiber reinforcement is an effective approach for enhancing the mechanical properties of composites [22, 23]. Due to their biocompatibility and mechanical strength, short silk fibers are often used as mechanically enhanced components for compounding with biomaterials such as gelatin and chitosan [24–26], but short silk fibers are simply dispersed [27, 28]. Here, we used silk short fibers to prepare mechanically enhanced silk fibroin scaffolds. To demonstrate the feasibility of this method, several key scientific questions need to be addressed: (1) How can composite scaffolds form stable crosslinking structures with enhanced mechanical properties and elastic properties? (2) How can a rapid, uniform and high-density distribution of cells in the composite scaffold be achieved? (3) How can structural stability and tissue homogeneity be sustained in the dynamic mechanical environment in vivo? The answers to these questions will not only promote the efficiency and quality of cell and scaffold integration but also produce important factors of regenerated tissue for clinical applications.

In the present study, we designed and synthesized a fiber-reinforced (Fr) silk fibroin (SF) super elastic absorbent sponge (SEAs) by employing a double network structure with multiple physical and chemical crosslinking mechanisms, endowing the scaffold with a superlight weight, good elasticity and fatigue durability. The Fr-SF-SEAs exhibited improved hydrophilicity, modulus, elasticity and stability compared to a pure SF-SEAs. By using two types of SEAs, we proposed a new cell inoculation mode with cyclic compression to rapidly obtain uniform regenerated tissue with a high cell density. Subsequently, star-shaped SF-SEAs and Fr-SF-SEAs were implanted subcutaneously in a nude rat model after chondrocyte inoculation with cyclic compression. At both 4 weeks and 8 weeks following scaffold implantation, morphology analyses, and histological assessments, we further showed that the Fr-SF-SEAs remarkably improved the structural stability, cellular uniformity and growth quality of regenerated cartilage. Moreover, the ear-shaped Fr-SF-SEAs showed a stable and precise ear-bionic structure for cartilage regeneration on a human scale. The results of this study regarding this novel Fr-SF-SEAs and cyclic compression cell inoculation mode are expected to be applied to the large-size regeneration of various tissues with better morphological stability and cellular uniformity.

Experimental Section

Silk Short Fiber Preparation

Silk short fibers were through the sodium hydroxide alkali hydrolysis of cocoons following previous protocols [29]. Briefly, the cocoons were cut into small pieces and placed in boiling 0.5% sodium carbonate solution (> 99.5%, Maclin) with stirring for 30 min and then washed thoroughly with deionized water for degumming. The above steps were repeated three times, and then the degummed silk fibers were dried in air. The dry degummed silk fibers (0.35 g) were added to 5 mL NaOH (> 96%, Sinopharm) aqueous solution (0.7 g/mL, w/v) with continuous stirring for the alkaline hydrolysis reaction. After stirring for 180 s, 45 mL of water was added to the reaction mixture to stop the hydrolysis. The reacted suspension was centrifuged and washed in water for 6 cycles to remove the excess remaining base. The pH was adjusted to 7.0 with hydrochloric acid (37%, Aladdin). The neutralized fiber solution was again centrifuged and resuspended in water for 5 cycles and then freeze-dried to obtain short silk fibers.

Fabrication of SEAs

Insoluble scaffolds of Fr-SF-SEAs (1:2) were fabricated with SF solution, short silk fibers, ethylene glycol diglycidyl ether (EGDE, epoxy value: ≥ 0.7, Macklin) and *N*,*N*,*N*',*N*'-tetramethylethylenediamine (TEMED, > 99%, Macklin). SF aqueous solution (5.0% w/v) was mixed with EGDE (3 mmol/g) and TEMED (0.25 v/v %) with continuous stirring in an ice bath. Then, the silk short fibers were added to the SF aqueous solution and uniformly mixed at a weight ratio of 1:2 (fiber/SF). The mixture was transferred into molds of different shapes (cylinder, cube, T-shape, star, flower, human ear), first for rapid freeze-setting at − 80 °C for 1 h, followed by a cryogen reaction at − 10 °C for 1 day, and then thawed at room temperature for 6 h. The reacted insoluble scaffolds were rinsed in ultrapure water to remove residual crosslinker and catalyst. Finally, the Fr-SF-SEAs (1:2) scaffolds were freeze-dried in vacuum. The pure SF-SEAs and Fr-SF-SEAs (2:2) were fabricated by the same method separately using different weight ratios of silk short fiber and SF at 0:2 and 2:2.

Scanning Electron Microscopy (SEM)

Sections of the scaffold and short silk fibers microstructures were observed with scanning electron microscopy (Zeiss Gemini 300) at an accelerating voltage of 10 kV. All samples were sputter-coated with gold before observation. To investigate the pore size of the scaffolds and the morphological characters of the fibers, the SEM image data were analyzed to evaluate the porous features inside of scaffolds and the parameters of short silk fibers using ImageJ software (ImageJ 1.53k, National Institute of Mental Health, Bethesda, MD).

Fourier Transform Infrared (FTIR) Spectroscopy

Attenuated total reflectance FTIR spectra of pure SF, pure fibers, crosslinked fibers, SF-SEAs and Fr-SF-SEAs were recorded with a spectrometer (Thermo Scientific Nicolet iS20) to identify the crosslinked groups of the SEAs. The FTIR spectra were recorded in the wavenumber range of 400–4000 cm^{-1} by accumulating 32 scans under a resolution of 4 cm^{-1}.

X-ray Diffraction (XRD)

With an X-ray diffractometer (Rigaku Smartlab 9KW), the crystallinity of the SF-SEAs, Fr-SF-SEAs (1:2) and Fr-SF-SEAs (2:2) was examined using Cu-K radiation (wavelength of 0.1542 nm) in step-scan mode in the 2 range of 5°-90° with a scanning speed of 2°/min. The X-ray diffractometer was operated at 30 kV and 30 mA. The test samples were made in the following ways. Using a sharp blade, the surface layers of the freeze-dried scaffold were removed. The remaining portion was then divided into slices that were 1 to 2 mm thick. The slices were finally compacted for the XRD test.

Porosity

The drainage method reported in a prior study was used to analyze the porosity of the SF-SEAs, Fr-SF-SEAs (1:2) and Fr-SF-SEAs (2:2) [30]. In brief, the weight of the dry scaffold ($n = 5$) was referred to as W_d, and the weight of the wet sample was referred to as W_w after the samples were entirely submerged in 100% ethanol. The scaffold porosity was then determined using the following formula:

$$\text{Porosity} = \left(W_w - W_d\right)/(\rho * V)\,100\%$$

where ρ and V denote the absolute ethanol density and scaffold volume, respectively.

Contact Angle

An optical water contact angle measurement system (Dataphysics OCA20) was used to analyze the wettability characteristics of the samples. Each sample with a diameter of 6 mm was placed on the surface to calculate the contact angle. A droplet of deionized water was deposited on the

sample using a 10 μL pipette tip and a high-resolution camera. Then, the image of the static liquid deposition was obtained within a few seconds and analyzed.

Water Absorption

The water absorption properties of the lyophilized SF-SEAs, Fr-SF-SEAs (1:2) and Fr-SF-SEAs (2:2) with the same size of 6 mm × 6 mm (diameter × thickness) were estimated on the basis of the change in weight in deionized water ($n = 5$). In brief, the dry scaffolds were weighed as W_0 before submersion in 5 mL phosphate-buffered saline (PBS) solution. After two hours of removal of excess PBS, the wet scaffolds were weighed. The water absorption of the scaffolds was calculated by the following equation:

$$\text{Water absorption ratio } (\%) = \left(W_1 - W_0\right)/W_0 * 100\%$$

W_0 was the dried weight before immersion in PBS, and W_1 was the wet weight of the hydrated scaffolds.

Mechanical Characteristics of Scaffolds

The mechanical properties of the scaffolds were determined using a mechanical testing machine (Instron-5542) as reported previously [31]. The SF-SEAs, Fr-SF-SEAs (1:2) and Fr-SF-SEAs (2:2) scaffolds were processed to a cylindrical shape that was 6 mm in diameter and 6 mm in thickness. To evaluate the properties of wet scaffolds, the three kinds of SEAs were placed in PBS at room temperature to equilibrate before testing. In the axial compression tests, the SEAs were compressed to a maximal strain of 50% at a rate of 10 mm/min ($n = 5$). The moduli were calculated by plotting the stress−strain curves. In the cyclic compression test, the specimens were compressed to a maximal strain of 60% for 10 cycles at a rate of 10 mm/min.

Chondrocyte Seeding and Culture of SEAs

In this study, all animals received humane care, in accordance with the National Institutes of Health Guide for the Care and Use of Laboratory Animals (NIH Publications No. 8023, revised 1978). The Shanghai Jiao Tong University Institutional Animal Care and Use Committee supervised all of the experimental operations. All samples were radiation sterilized for subsequent tests.

As previously reported, auricular cartilage was obtained from rabbits and cut into 1.0 mm pieces before being washed with phosphate-buffered saline (PBS) and digested with 0.15% collagenase (Worthington Biochemical Corp., NJ, United States) to isolate chondrocytes [32]. The isolated chondrocytes were cultured in Dulbecco's modified Eagle's medium (DMEM) containing 10% fetal bovine serum (Gibco BRL, Grand Island, NY, USA) and 1% antibiotic–antimycotic solution (Gibco BRL).

A 100 μL cell suspension (6×10^7 cells/mL) of P2 chondrocytes was seeded into the SF-SEAs and Fr-SF-SEAs (1:2) scaffolds. Two inoculation methods were chosen to seed the cells, which were divided into the drip infiltration (DI) group and cyclic compression (CC) group as follows:

DI group: Using a pipette gun, the cell suspension was slowly dropped onto the SEAs scaffold surface until it was completely absorbed.

CC group: The cell suspension was first infiltrated into the SEAs scaffold using the same method as the DI group, and then the SEAs scaffolds were gently squeezed with sterile forceps to produce partial deformation and released to the original shape, and each scaffold was cyclically compressed ten times.

Cell seeding efficiency at 4 h was used to assess cell absorption ability using an established calculation protocol [33].

Cell Distribution of SEAs

Following 7 days of culture, samples were cut along the longitudinal direction and stained with 4′,6-diamidino-2-phenylindole (DAPI) to assess the uniformity of cell distribution. For the other SEAs samples, four aliquots were set according to their height and cut horizontally along the aliquots, and the quartile point horizontal sections (i.e., representing the inoculum depth) were assessed using the Live and Dead cell viability assay (Invitrogen, USA) according to the manufacturer's instructions. For each section, living cells were counted and reported as the mean number per high power field (HPF) ($n = 9$).

In addition, DNA content was used to further assess the total number of cells in each sample ($n = 5$) using a total DNA quantification assay (PicoGreen dsDNA assay, Invitrogen, USA).

Subcutaneous Implantation and Morphological Analysis

Four-week-old nude mice (Shanghai Jiagan Biological Technology Co., Shanghai, China) were used in this study. Star-shaped SF-SEAs and Fr-SF-SEAs (1:2) were seeded with 1.2×10^7 (200 μL, 6×10^7 cells/mL) chondrocytes by the cyclic compression method. All specimens were grown in chondrogenic-inductive media contained several components, including transforming growth factor beta-1 (TGF-1), insulin-like growth factor-I (IGF-I), and other supplements [34]. After 2 weeks of in vitro culture, engineered cartilage with a certain level of maturity was formed by regeneration. Then, they were subcutaneously implanted in nude mice for

4 and 8 weeks to form regenerated cartilage tissues at different stages of maturation in vivo ($n=5$). All specimens were carefully stripped of the surrounding connective tissue, and overall images were collected at different time points to measure the projected area for further analysis [35]. The Edge deformation of the regenerated tissue was estimated based on the thickness change of the pentagonal regenerated cartilage ($n=5$). Briefly, the thickness of each corner of the pentagonal regenerated cartilage tissue was measured and its thickness was recorded as H_0. In measuring the thickness of the center of the regenerated tissue, it was recorded as H_1. The edge deformation of the regenerated tissue was calculated according to the following equation:

$$\text{Edge deformation}\ (\%) = \left(H_1 - H_0\right)/H_0 * 100\%$$

Biomechanical and Biochemical Analysis

The regenerated star-shaped cartilage was collected in vivo, and its weight and volume were recorded; it was then used for biomechanical and biochemical studies. The strain–stress curve and modulus of the regenerated cartilage were measured using a mechanical analyzer (Instron-5542). Specimens from both groups were chopped for the quantitative analysis of glycosaminoglycan (GAG), collagen content and elastin content ($n=5$), as previously described [36, 37].

Histological Analyses

To evaluate the quality of regenerative cartilage tissue, all engineered tissues harvested above, were subjected to histological and immunohistochemical examinations as described previously [38]. The regenerated star-shaped cartilage samples were sectioned into 5 μm slices for staining. Hematoxylin and eosin (H&E) staining, safranin-O (SO) staining, and the immunohistochemical staining of type II collagen (COL II) were performed to observe the histological structure and cartilage matrix deposition of GAG and COL II, respectively. Briefly, samples were fixed in 4% paraformaldehyde, embedded in paraffin, and sectioned. Then, sections were stained with H&E and safranine-O. The expression of type II collagen was detected using a mouse monoclonal antibody against collagen II (MS-306-P1, 1:200, Invitrogen, USA), followed by a horseradish peroxidase-conjugated anti-mouse antibody (1:200, Dako, Denmark). Both antibodies were diluted in PBS and then colorized with diaminobenzidine tetrahydrochloride (DAB, Dako).

Construction of Ear-Shaped Cartilage

To explore the long-term fate of the regenerated tissues of large-scale SEAs, we chose to construct human ear-shaped Fr-SF-SEAs (1:2) scaffolds with a silicone mold. The large-scale ear-shaped Fr-SF-SEAs (1:2) ($n=5$) were subjected to cyclic compressed inoculation with 9×10^7 (1.5 mL, 6×10^7 cells/mL) cells, cultured in vitro in cartilage for 2 weeks, and then implanted into nude mice for 6 weeks and 12 weeks. The human ear-shaped engineered tissues were harvested and then subjected to histological and immunohistochemical examinations as described above.

Statistical Analysis

Data were analyzed with SPSS software. $^*P<0.05$ was considered significant. All values are reported as the means ± standard deviations.

Results

Fabrication and Morphology of SEAs

We created three kinds of SEAs: SF-SEAs, Fr-SF-SEAs (1:2) and Fr-SF-SEAs (2:2) containing only SF, and fiber/SF (1:2) and fiber/SF (2:2) with different ratios of SF and silk short fibers. The length of silk microfibers formed during the hydrolysis process was related to the period of hydrolysis. After 180 s of alkaline hydrolysis reaction, the silk short fibers was obtained with length of 164 ± 75 μm and diameter of 13 ± 2 μm (Supplementary Fig. S1). When different proportions of the two components were dissolved and dispersed in deionized water, it was macroscopically observed that the SF solution was homogeneous. Although Fr-SF (1:2) suspension appears slightly uneven mixture, the Fr-SF (1:2) was more uniform than the Fr-SF (2:2) suspension which showed obvious undesirable settle and stratify (Fig. 1b). Similar results were obtained for the SEAs scaffolds fabricated by crosslinking and lyophilizing. The SF-SEAs and Fr-SF-SEAs (1:2) scaffolds had smooth and uniform surfaces, but the Fr-SF-SEAs (2:2) had uneven surfaces due to the high content of fiber with inhomogeneous dispersion (Fig. 1c). The SEAs were prepared into various complex morphologies by using different molds (Fig. 1d). Due to the high porosity of the scaffolds, the Fr-SF-SEAs had an ultralight structure (Fig. 1e).

SEM images (Fig. 1f) showed that the SEAs all had interconnected micropore structures. The SF-SEAs had larger pores (320.96 ± 102.64 μm) and smooth pore walls. The Fr-SF-SEAs (1:2) and Fr-SF-SEAs (2:2) exhibited embedded and crosslinked silk short fibers, with the pore size decreasing (45.89 ± 13.76 μm, 39.15 ± 16.08 μm) as the fiber content increased (Fig. 1g). At low magnification, the pure SF SEAs and Fr-SF-SEAs (1:2) exhibited abundant homogeneous micropores in whole scaffold. But the Fr-SF-SEAs (2:2) existed obvious fiber aggregation that resulted in

unsatisfactory inhomogeneous microstructures (Supplementary Fig. S2). Moreover, the SEM images of Fr-SF-SEAs (1:2) in sectional views from top to bottom also demonstrated similar and regular microstructures in different parts (Supplementary Fig. S3). FTIR spectroscopy of the silk protein, short fiber, crosslinked SF-SEAs and crosslinked Fr-SF-SEAs showed that the amide I absorption bands of the crosslinked SEAs both shifted to a lower wavenumber (Fig. 1h). This proved the dual crosslinking of EGDE with SF and silk fibers. X-ray diffraction (XRD) showed a typical peak at 20.4° for all three kinds of SEAs, which is the characteristic peak for the β-folded crystal structure of silk protein chains (Fig. 1i).

Hydrophilicity and Mechanical Properties

The wet Fr-SF-SEAs (1:2) resisted multiple compression deformations well, and its original structure was able to be restored under the dynamic stress effect (Fig. 2a, and Video S1). The average porosities of the SF-SEAs, Fr-SF-SEAs (1:2) and Fr-SF-SEAs (2:2) were $96.13 \pm 2.08\%$, $89.77 \pm 4.16\%$ and $87.73 \pm 3.38\%$, respectively (Fig. 2b).

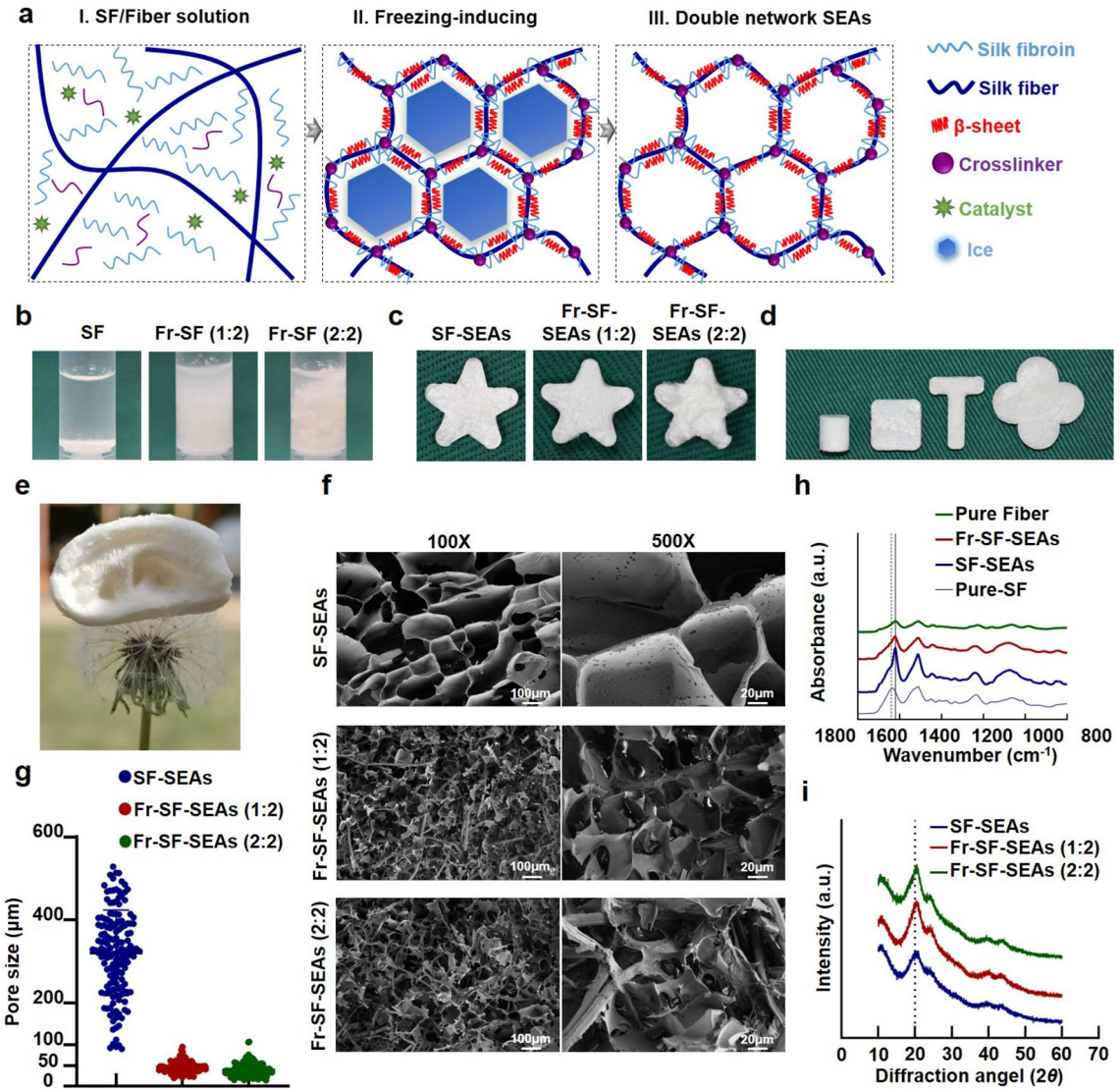

Fig. 1 Design of the Fr-SF-SEAs scaffolds. **a** Ice crystal growth in the fiber/SF solution and induction of phase separation under freezing conditions. The β-sheet of SF molecular chains and epoxy-amino/hydroxyl reactions of SF and fibers form the physical and chemical double-crosslinking network. **b** Mixed suspensions of SF solution and silk short fibers in different proportions. **c** Images of the star-shaped SF-SEAs, Fr-SF-SEAs (1:2) and Fr-SF-SEAs (2:2). **d** Fr-SF-SEAs (1:2) with different morphologies. **e** Superlight human-scale ear-shaped Fr-SF-SEAs (1:2) placed on dandelion fluff. **f** SEM images of SEAs sections at different magnifications. Scale bars: 100 μm and 20 μm. **g** Micropore size distribution of SEAs. **h** FTIR spectroscopy analysis of the crosslinked groups of SEAs. **i** XRD patterns of SEAs for crystalline structure analysis

The initial contact angles of the Fr-SF-SEAs (1:2) and Fr-SF-SEAs (2:2) composite scaffolds were slightly higher than that of the SF-SEAs, but the droplets were absorbed significantly faster into the scaffolds (Fig. 2c, d). The SF-SEAs, Fr-SF-SEAs (1:2) and Fr-SF-SEAs (2:2) showed high hydroscopicities with maximum water absorptions of 1,678 ± 19%, 1,413 ± 38% and 1,013 ± 24%, respectively (Fig. 2e).

On the other hand, adding short fibers significantly enhanced the compressive resistance of the scaffolds. The uniaxial compression tests showed that the SF-SEAs, Fr-SF-SEAs (1:2) and Fr-SF-SEAs (2:2) had moduli of 16.31 ± 1.01, 41.22 ± 1.40 and 46.82 ± 2.04 kPa, respectively (Fig. 2f, g). Furthermore, cyclic compression tests showed that the SF-SEAs, Fr-SF-SEAs (1:2) and Fr-SF-SEAs (2:2) had superior elasticity and antifatigue properties with limited hysteresis under dynamic pressure (Fig. 2h). The addition of fibers to the SF-SEAs enabled an increase in the strength restoration after the 1st cycle from the 2nd to 10th cycles, which revealed that the Fr-SF-SEAs (1:2) and Fr-SF-SEAs (2:2) had better recoverability than the SF-SEAs (Fig. 2i). By comprehensively considering the structural uniformity, surface precision, hydrophilicity and mechanical properties, the Fr-SF-SEAs (1:2) was selected for comparison with the SF-SEAs in further studies.

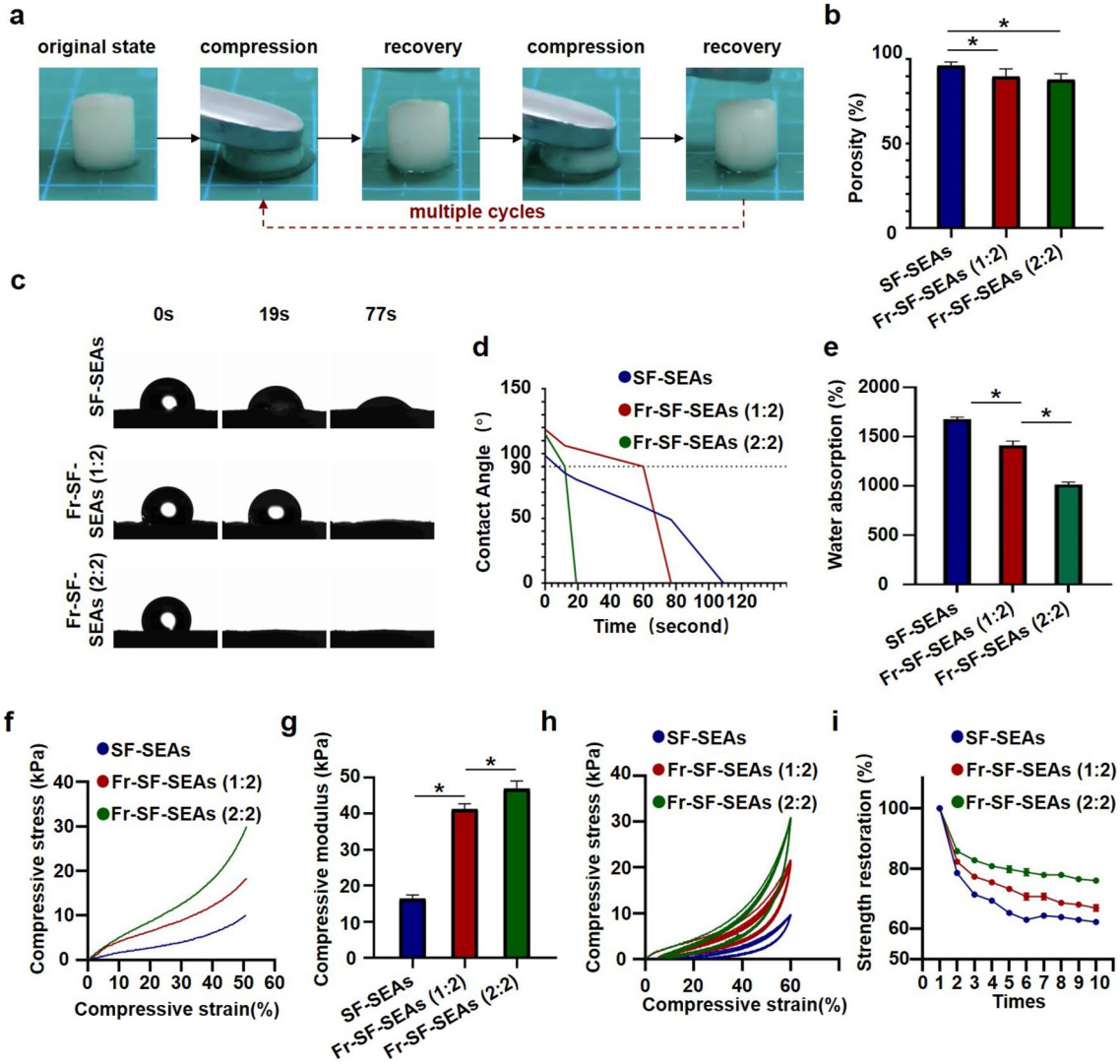

Fig. 2 Characterization of the SEAs. **a** Time-lapse images of the deformation and restitution of the wet Fr-SF-SEAs (1:2) over multiple cycles. **b** Porosity of SEAs scaffolds with different ratios. **c** Recorded images of the dynamic contact angle of SEAs at different times. **d** Change curves of the contact angle versus time. **e** Water absorption capacity of the SEAs. **f** Typical compressive stress−strain curves of the wet SEAs. **g** Comparison of the compressive modulus. **h** Cyclic compression tests of the wet SEAs for 10 cycles with a maximum strain of 60%. **i** Comparison of the dynamic compress strength restoration of the SEAs at a strain of 30% from the 2nd to 10th cycles compared to the 1st cycle. (*$P < 0.05$)

Cell Inoculation and Distribution of the SEAs

Once the porous scaffold composition was optimized, evaluating the scaffold seeding behaviors during regeneration became the focus of this study. We treated the SF-SEAs and Fr-SF-SEAs (1:2) with different methods of cell seeding by drip infiltration (DI) (Fig. 3a1), and cyclic compression (CC) (Fig. 3a2), respectively. Cytotoxicity assays were performed to evaluate the biocompatibility of these scaffolds, as well as their cell seeding efficiency, DAPI staining, cell viability, and DNA content, to evaluate the effectiveness of cell inoculation. The cytotoxicity analysis of the leachates verified that cell proliferation in the SF-SEAs and Fr-SF-SEAs (1:2) groups was significantly higher than that in the regular group (Fig. 3b). The results of the cell seeding efficiency revealed that in each group, the cell seeding efficiency was more than 90%, the Fr-SF-SEAs (1:2) were significantly superior to the SF-SEAs, and the efficiency of inoculation after cyclic compression was significantly higher than that after drip infiltration (Fig. 3c). After 1 week of in vitro culture, the scaffolds were cut into different slices to analyze the effect of inoculation, and the sections were selected as shown in Fig. 3d1–d4. Some of the scaffolds were incised longitudinally, and the cell distribution was observed with DAPI staining (Fig. 3e1, f1, g1 and h1). The cells were more uniformly distributed in the circulatory compression (CC) mode than in the drop inoculation (DI) mode, in which the cells tended to be distributed more superficially in the scaffold. Moreover, the rest of the scaffolds were cut horizontally from the upper, middle and lower levels, and live & dead staining was used to observe the cell viability and density at different levels (Fig. 3e2–e4, f2–f4, g2–g4, h2–h4). These results revealed that the Fr-SF-SEAs (1:2) CC group achieved a more uniform distribution and higher density of inoculation (Fig. 3i, j). DNA quantitative analysis further indicated that the Fr-SF-SEAs (1:2) had a better performance (Fig. 3k).

Morphological Stability of Star-Shaped Regenerated Cartilage

To assess the advantage of fiber-reinforced SEAs scaffolds in terms of shape maintenance, SEAs were prepared in the complex shape of a star with well-defined edges and corners, and chondrocytes were inoculated onto Fr-SF-SEAs (1:2) and SF-SEAs. After two weeks of in vitro incubation, they were implanted subcutaneously into the backs of nude mice with a tight skin fit for analysis at 4 and 8 weeks. When the samples were taken, it was observed that each sample retained the smooth ivory appearance of the cartilage, and the shape remained similar to the original shape. Overall, the cartilage surface of the SF-SEAs group was obviously granular and heavily deformed at the edges; the surface of the Fr-SF-SEAs (1:2) group was smoother and flatter (Fig. 4a–d). As shown in Fig. 4e, the subcutaneous tension applied to the regenerated tissue was mainly applied to the marginal part, which was the main reason for the deformation.

During the growth of regenerated tissues in vivo, the wet weight and total volume of tissues steadily increased due to matrix secretion (Fig. 4f, g). Quantitative analyses of the projection regions in the top view and the thickness in the side view are shown in Fig. 4h, i. During 4 weeks and 8 weeks of in vivo growth, the SF-SEAs and Fr-SF-SEAs (1:2) both slightly changed shape in the top view with final deformation rates of 2.4% and 2.9% (Fig. 4h). The side view images showed that the regenerated cartilage of Fr-SF-SEAs (1:2) had a better consistency of thickness at different time points than the cartilage of SF-SEAs (Fig. 4i). Importantly, the cartilage of Fr-SF-SEAs (1:2) exhibited more significant uniform thickness in both the surrounding area and central area than the cartilage of SF-SEAs, indicating that the Fr-SF-SEAs (1:2) could maintain the original precise structure (Fig. 4j).

Histological Assessment of the Star-Shaped Regenerated Cartilage

Histological examination of the horizontal sections of the regenerated stellate cartilage in the two groups showed that typical cartilage trap structures became more pronounced and the scaffold became progressively degraded as the culture time increased. Enhanced GAG deposition and type II collagen expression were visualized with safranin-O and immunohistochemical type II collagen staining (Fig. 5a, b). This result was corroborated by quantitative biochemical analysis. Further observation of the high magnification field of histology showed that SF-SEAs showed poor maintenance of the precise structure and tended to atrophy (Fig. 5a2–a4, c2–c4). The exquisite structure of cartilage tissue regenerated by the fiber-reinforced scaffold was more completely preserved (Fig. 5b2–b4, d2–d4). It is also noteworthy that during the 4 weeks of growth and development, specimens of SF-SEAs still had void structures in the internal regions (Fig. 5a5–a7). In contrast, the Fr-SF-SEAs (1:2) samples containing short fiber components had abundant extracellular matrix growth between the fibrous-protein pore walls (Fig. 5b5–b7). After up to 8 weeks of incubation, the differences gradually decreased (Fig. 5c5–c7, d5–d7). This indicates that scaffolds containing fibrous components have a higher affinity, which contributes more to the homogeneous growth of the regenerated tissue. Although this difference can be eliminated later in the tissue regeneration process, the initial post implantation period, as the prime time for tissue growth, with a homogeneous distribution of cells as well as a full and secreted extracellular matrix, is crucial for resisting external stress and maintaining the shape of the regenerated tissue. Residual scaffold components can also

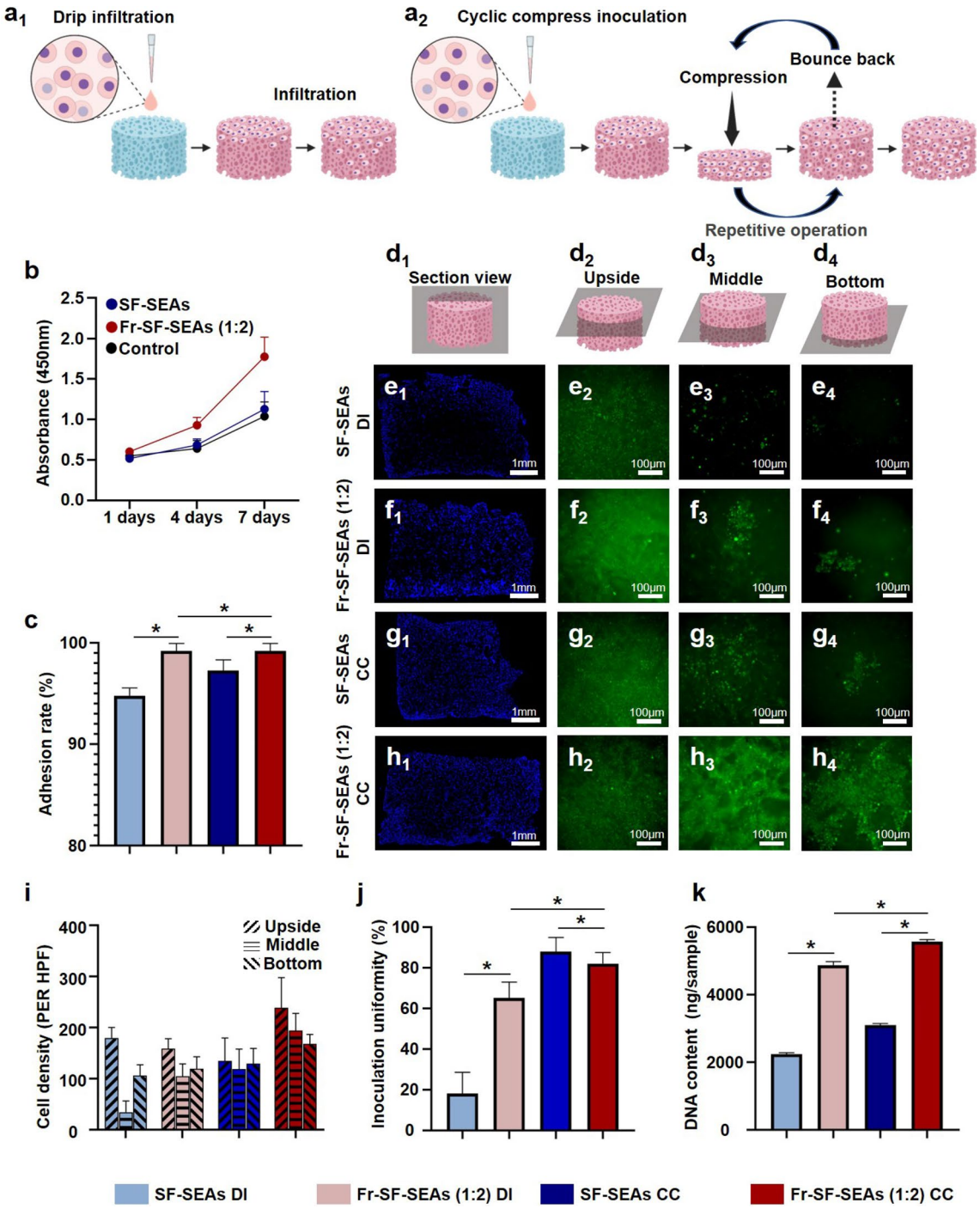

Fig. 3 Cyclic compression inoculation and cell distribution of the SEAs. $\mathbf{a_1}$, $\mathbf{a_2}$ Schematic diagram of the process of cell seeding by drip infiltration and cyclic compression inoculation method. **b** CCK-8 assay of chondrocytes seeded with the SF-SEAs and Fr-SF-SEAs (1:2) at 1, 4, and 7 days. **c** Cell seeding efficiency. $\mathbf{d_1}$–$\mathbf{d_4}$ Schematics of the cut sections. $\mathbf{e_1}$-$\mathbf{e_4}$ DAPI staining of the longitudinal section and live and dead staining of the quartile point horizontal sections of the SF-SEAs DI group. $\mathbf{f_1}$-$\mathbf{f_4}$ DAPI staining of the longitudinal section and live and dead staining of the quartile point horizontal sections of the Fr-SF-SEAs (1:2) DI group. $\mathbf{g_1}$-$\mathbf{g_4}$ DAPI staining of the longitudinal section and live and dead staining of the quartile point horizontal sections of the SF-SEAs CC group. $\mathbf{h_1}$-$\mathbf{h_4}$ DAPI staining of the longitudinal section and live and dead staining of the quartile point horizontal sections of the Fr-SF-SEAs (1:2) CC group. **i** Number of chondrocytes visible via high magnification. **j** Ratio of the number of cells in the middle layer to that in the inoculated upside layer. **k** DNA content of each sample measured 7 days after cell seeding. (DAPI staining: scale bar = 1 mm; live and dead staining: scale bar = 100 μm; $^*P < 0.05$)

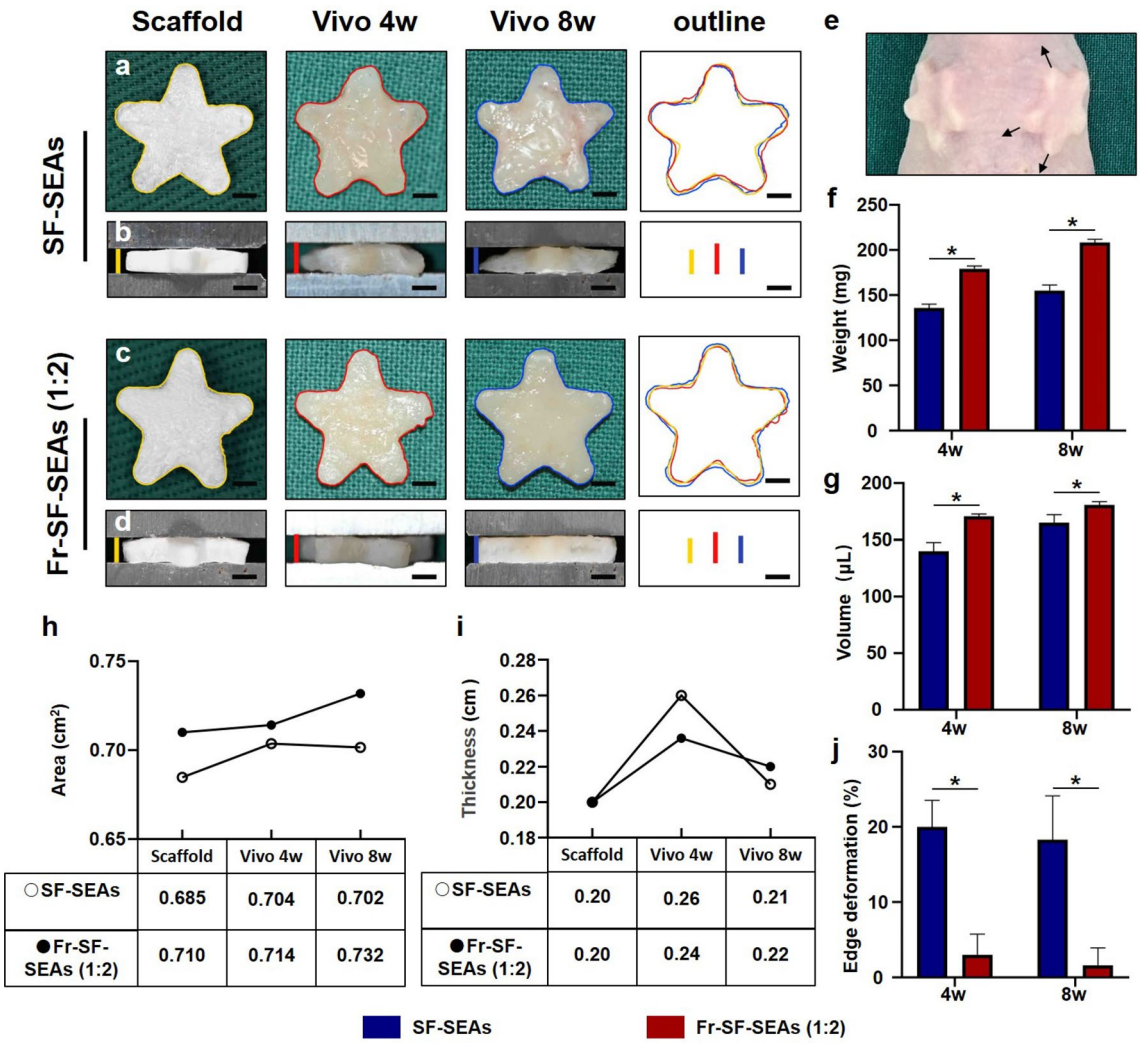

h	Scaffold	Vivo 4w	Vivo 8w
○SF-SEAs	0.685	0.704	0.702
●Fr-SF-SEAs (1:2)	0.710	0.714	0.732

i	Scaffold	Vivo 4w	Vivo 8w
○SF-SEAs	0.20	0.26	0.21
●Fr-SF-SEAs (1:2)	0.20	0.24	0.22

Fig. 4 Shape analysis of star-shaped SEAs and regenerated cartilage tissues at 4 weeks and 8 weeks after subcutaneous implantation. **a–d** Morphologies of the SEAs and their star-shaped regenerated cartilage tissues in top view and side view. Scale bar = 2 mm. **e** Gross view of star-shaped cartilages under the nude rat skin. **f** Weight and **g** volume of regenerated cartilage. **h, i** Projection area in top view and thickness of the SEAs scaffolds and regenerated cartilage tissues. **j** Degree of deformation in the edge region of the SEAs after in vivo implantation. (*$P < 0.05$; the black arrows denote the direction of subcutaneous tension)

be seen in the internal region of the specimen (Fig. 5a5, b5, c5, d5). At 4 weeks there is more residual scaffold, which is easily detected; by the time the scaffold has largely degraded after 8 weeks in vivo incubation, there is less residual component. SEAs exhibit an appropriate rate of degradation for better cell interactions and tissue repair in vivo. Combining the above experimental results, it can be confirmed that the mechanical strength of the Fr-SF-SEAs (1:2) is sufficient for coping with the taut environment of subcutaneous growth and has better performance in terms of shape fidelity.

Quantitative analysis further supported the gross observation and histology findings. The elastic cartilage-specific extracellular matrix (ECM) contents (e.g., total collagen, GAG, and elastin) demonstrated gradually increasing trends, indicating that the in vivo environment facilitated improvement in cartilage regeneration. (Fig. 5e–g). Compared with the SF-SEAs group, whose regenerated cartilage had a modulus of 0.615 ± 0.03 MPa and 1.38 ± 0.07 MPa at 4 weeks and 8 weeks after subcutaneous implantation, the Fr-SF-SEAs (1:2) group had regenerated cartilage with a significantly increased modulus of 1.60 ± 0.11 MPa and 3.10 ± 0.17 MPa (Fig. 5h). The quantitative biochemical and biomechanical results between the Fr-SF-SEAs (1:2) and SF-SEAs groups also showed statistically significant

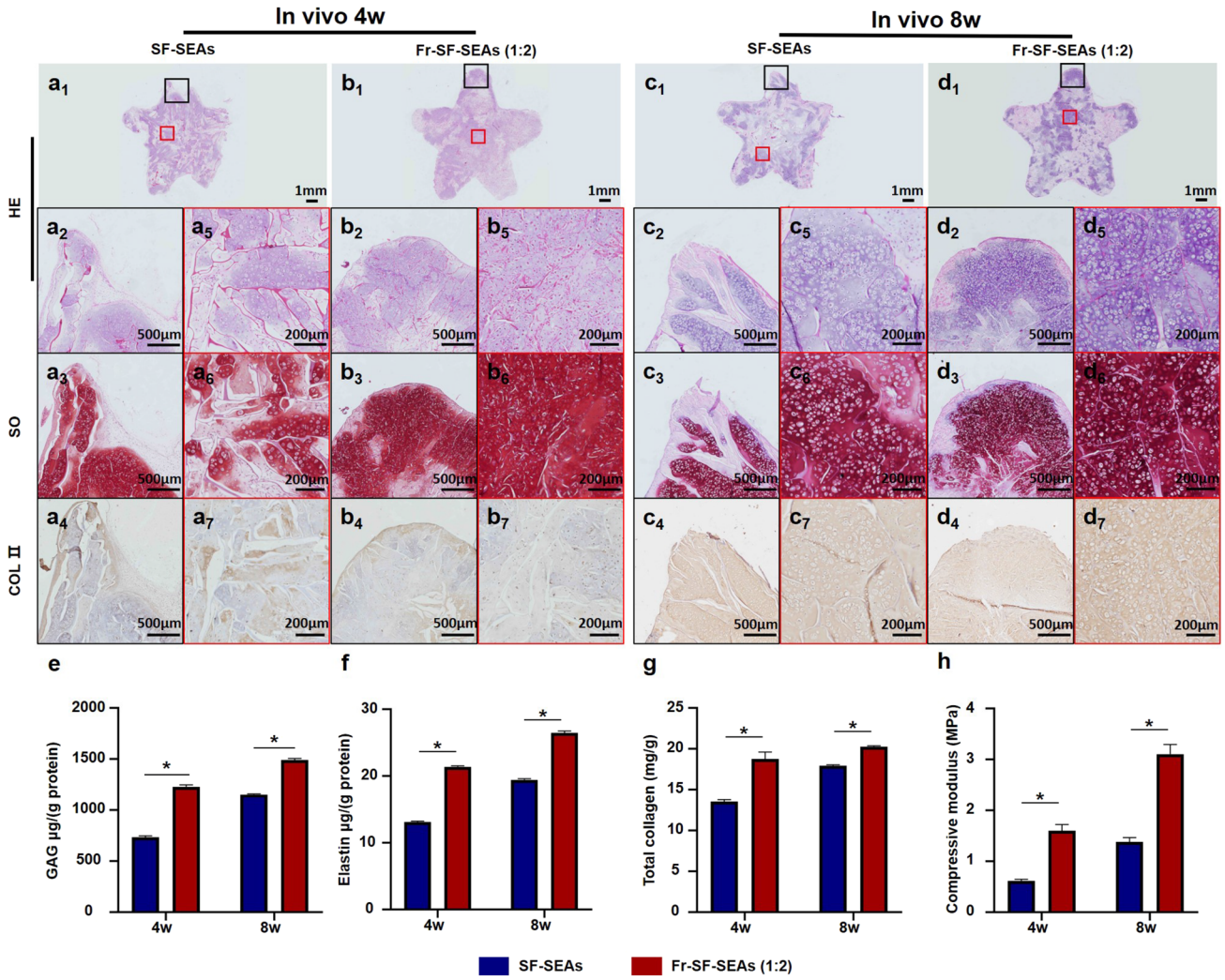

Fig. 5 Histological and quantitative evaluations of the star-shaped regenerated cartilage at 4 weeks and 8 weeks after subcutaneous implantation. H&E, Safranin-O and collagen II immunohistochemical staining of SF-SEAs ($\mathbf{a_1}$–$\mathbf{a_7}$, $\mathbf{c_1}$–$\mathbf{c_7}$) and Fr-SF-SEAs (1:2) ($\mathbf{b_1}$–$\mathbf{b_7}$, $\mathbf{d_1}$–$\mathbf{d_7}$) constructs. **e** Total glycosaminoglycan (GAG), **f** elastin and **g** total collagen contents. **h** Young's modulus. (Scale bars = 1 mm, 500 μm and 200 μm; the black box represents the marginal areas of cartilage tissue, and the red box represents the central areas of cartilage tissue; $^*P < 0.05$)

differences, and the regenerated cartilage tissue in the Fr-SF-SEAs (1:2) group behaved more maturely, indicating that the addition of the fibrous component had a positive effect on the formation of cartilage.

Human-Scale Ear-Shaped Cartilage Regeneration

To further evaluate the feasibility of the Fr-SF-SEAs (1:2) to achieve large and finely shaped tissue regeneration and then expand the application prospects of SEAs, we reconstructed human ear-shaped cartilage in a nude mouse model, which is noteworthy. Human ear-shaped cartilage has been a challenge for clinical translation due to its large volume and certain morphological structural requirements. In this study, a scaffold of Fr-SF-SEAs (1:2) in the shape of human ear was prepared using the selected silicone mold infusion molding method (Fig. 6a), which allowed easy and precise customization of the three-dimensional shape. The ear-shaped Fr-SF-SEAs (1:2) exhibited excellent elasticity and recoverability in the wet state (Video S2). After 2 weeks of in vitro culture, the original shape was maintained with a precise structure (Fig. 6b, Video S3). Then, the ear-shaped regenerated cartilage was implanted subcutaneously in nude mice, and the clear auricular structure was immediately visible after the negative pressure aspiration of residual gas (Fig. 6c). After 12 weeks of in vivo culture (Video S4), the Fr-SF-SEAs (1:2) successfully regenerated human ear-shaped cartilage tissue with a stable intraauricular structure, in contrast to the SF-SEAs constructed ear, which lost its original shape (Video S5).

After 6 weeks, the gross appearance did not change significantly, the auricular cavity was well defined, and histological findings showed that the ear-shaped structures initially formed cartilage-like tissues with typical void structures and cartilage-like features (Fig. 6d). Staining revealed the presence of widely distributed cartilage ECM. However, the maturity of the regenerated tissue was not yet satisfactory, and immature cartilage was still observed in the region of the regenerated cartilage center (Fig. 6f). At 12 weeks (Fig. 6e), the cartilage-like tissue of the constructs was more mature with abundant gap structures and homogeneous cartilage ECM distribution, and the positive staining for GAG and COL II expression was stronger, which showed that in vivo cartilage regeneration underwent a gradual maturation process (Fig. 6g). Compared with the previous deficiencies in large tissue-engineered cartilage regeneration, in which the maturation of deep cells was much lower than that of the superficial region, signs of deep chondrocytes reaching maturity was observed in histological sections at either 6 or 12 weeks. What was not difficult to observe was that the pore distribution of the scaffold was oriented such that the structure was more conducive to nutrient perfusion into the deeper tissues, which was clearly evidenced by the distribution of ECM in the histology. The combined results suggested that Fr-SF-SEAs (1:2) have the potential to achieve large tissue regeneration in the field of tissue engineering.

Discussion

Here, we report a novel fiber-reinforced silk fibroin super elastic absorbent sponge, called Fr-SF-SEAs (1:2), which has an improved uniform cell distribution and demonstrates an enhanced shape fidelity of regenerated tissue. The Fr-SF-SEAs (1:2) were synthesized with a double network structure by physical and chemical crosslinking. The SF network consisted of β-sheet physical crosslinking and catalytic chemical crosslinking with an epoxide crosslinker (EDGE). The epoxide groups on both ends not only combined with the amino and hydroxyl groups on SF but also reacted with the amino and hydroxyl groups on the SF fiber surface to build a fiber crosslinking network (Fig. 1a). Using this general strategy, many other proteins, such as collagen and decellularized matrix, can be introduced into the double-crosslinking network system to build bioactive SEAs. SEAs can be easily fabricated with various geometries and ultralight structures to match different tissue defects. Ice templating allows the interconnected honeycomb structure of the SEAs to have a high porosity, which is beneficial for cell adhesion, growth and survival. The fibers were embedded and distributed in the SEAs to connect the adjacent micropores, and this fiber network might provide guiding channels for cell infiltration and migration. With the addition of fibers, the micropore size significantly decreased from hundreds of micrometers to several tens of micrometers because the fibers inhibited the formation of ice crystals. The smaller micropores of the Fr-SF-SEAs (1:2) were slightly larger than the cell size, and once the cells infiltrated into the inner Fr-SF-SEAs (1:2), they were captured and not easily lost.

The SEAs exhibited stiff properties in the dry state and rapidly became soft in the wet state due to the hydrogen bonding interactions and hydrophilicity of the abundant amino and hydroxyl groups. The Fr-SF-SEAs (1:2) had a smaller micro/nanostructure than the SEAs that resulted in a higher initial contact angle. However, the Fr-SF-SEAs (1:2) absorbed water more quickly because of the existence of fiber, which functioned as a drainage channel to induce water infiltration. Although fiber addition caused a decrease in porosity, the Fr-SF-SEAs (1:2) still showed excellent water absorption ability. With the increase in the short fiber content, the stiffness and mechanical strength of the SEAs increased with the modulus from a dozen to several tens of kPa. Due to the stable double-crosslinking network, the Fr-SF-SEAs (1:2) exhibited better elasticity and fatigue durability to withstand multiple deformations and maintain its original structure during dynamic cell seeding. The soft and flexible Fr-SF-SEAs (1:2) was compressed into a small size to discharge the inner liquid, then the excellent structural restoration and siphonage effect allowed the cell suspension to be absorbed, and the cells were most likely captured in the internal micropores. Overall, the complementary design resulted in a SEAs scaffold with comprehensive, synergistic effects, such as suitable micropores, hydrophilicity, elasticity and enhanced mechanical properties, to enable cyclic compression cell seeding and large-scale tissue regeneration.

The effectiveness of cell inoculation is one of the most important influencing factors, for characterizing the quality of tissue-engineered regenerated tissues [39]. In this study, a dual-network system could significantly improve cell inoculation efficiency. On the one hand, the elastic SEAs could be repeatedly compressed and recovered in dynamic cell inoculation. The sponge-like pressure-suction characteristics actively increasing the number and rate of cell spreading so that more cells can be absorbed and evenly distributed to the whole scaffold. On the other hand, the adding fibers played an important role in enhancing cell infiltration. First, the fibers increased the hydrophilicity of scaffold that facilitated the cell absorption. Second, cells need pass through several pores to penetrate into a certain depth in SF-SEAs scaffold, but the embed fibers could serve as drainage channels to shorten cell diffusion path, and the cell could more easily penetrate inside of Fr-SF-SEAs (1:2). Third, although the pore size of Fr-SF-SEAs (1:2) was obviously smaller than SF-SEAs, the cell inoculation efficiency of Fr-SF-SEAs (1:2) was higher than SF-SEAs. The pore size of SF-SEAs

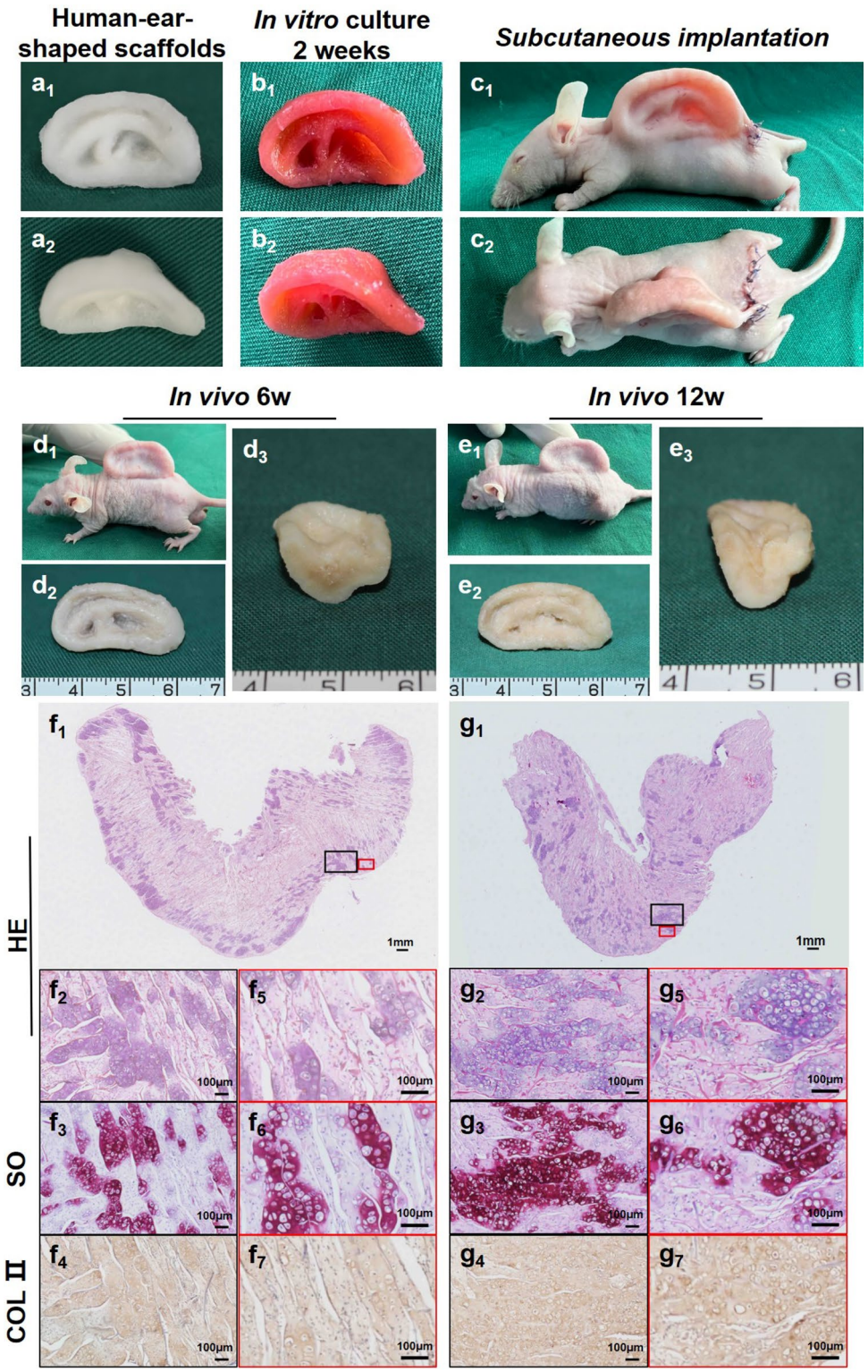

Fig. 6 In vivo regeneration of human-scale ear-shaped cartilage. **a** Human-ear-shaped Fr-SF-SEAs (1:2) scaffold. **b** Maintaining the original shape and size after 2 weeks of in vitro culture. **c** Subcutaneous implantation of tissue-engineered cartilage into nude mice. **d, e** General appearance and cross-sectional view of the regenerated ear cartilage at 6 weeks and 12 weeks after in vivo implantation. **f, g** Immunohistochemical staining of regenerated ear cartilage with H&E, safranin-O and collagen II. Scale bars = 1 mm and 100 μm; the black box represents the marginal areas of cartilage tissue, and the red box represents the central areas of cartilage tissue

scaffold was too large to holding cell, and the pore size of Fr-SF-SEAs (1:2) was slightly larger than cell diameter that enabled to lock cell and decrease loss rate. It is also worth noting that the Fr-SF-SEAs (1:2) had a higher specific surface area, which is also more beneficial for cell adhesion and proliferation.

How to maintain the shape of structures with high fidelity in long-term culture is an urgent issue in tissue engineering, which is crucial for the clinical translation of tissue engineering research [40]. In this study, Fr-SF-SEAs (1:2) were incubated in vivo in a subcutaneous high-tension environment, and no signs of regression were observed with regard to the original shape, showing an excellent shape maintenance ability. Mechanical strength tests, quantitative analyses of two-dimensional area and scaffold height variations, and even three-dimensional shape observation revealed the same conclusion. From the perspective of composite mechanics, the incorporation of short fibers has been shown to significantly increase the mechanical properties of the scaffolds [41, 42], and the high load-bearing capacity of the filamentous short fibers and the interfacial interaction between the filamentous proteins and the reinforcing short fibers also play important roles in morphology maintenance, while on the other hand, the fiber fille's high water absorption capacity promotes the recovery of the scaffolds following deformation in a humoral environment [43]. From the perspective of cell-to-tissue growth and development, repeated squeezing and aspiration of the Fr-SF-SEAs (1:2) can significantly improve the homogeneity of cell inoculation, and the secreted ECM of the homogeneously grown cells can also evenly fill the interior of the scaffold, which has been reported to play an important role in supporting and stabilizing the structure of tissues [44, 45], such that the homogeneously produced ECM can assist in retaining form even as the scaffold gradually dissolves throughout development.

The further goal of this study was to determine whether the Fr-SF-SEAs (1:2) could be used for the regeneration of large-volume tissues. Here, we chose a large-volume ear reconstruction model to address the specific challenges of ear reconstruction in patients with clinical microtia. First, we prepared a mold with the shape of a human ear using silicone inversion molds, which were eventually molded by infusion, which allows for a simple solution to the problem of shaping and is generally applicable for all types of complex shapes. Then, chondrocytes were inoculated with ear-shaped Fr-SF-SEAs (1:2) scaffolds, which were subcutaneously replanted and finally successfully regenerated into bionic ear-shaped cartilage with mature quality. In our previous studies, poly(ε-caprolactone) was often taken as the internal support skeleton, and the slowly degrading poly(ε-caprolactone) occupied too much space, which affected the formation and integration of engineered cartilage and was a problem that we had been expecting to solve. In the present study, it was shown that relying on the incorporation of reinforcing fiber fillers allowed large-volume shape support and provided sufficient mechanical strength to cope with the subcutaneous tension environment. Moreover, compared to the coarser diameter support skeleton, the incorporated short fibers had a filamentous morphology similar to that of the collagenous protofibrils found in cartilage ECM, which can mimic the ultrastructure of cartilage ECM to a certain extent. Overall, the Fr-SF-SEAs (1:2) has great potential for regenerative tissue applications.

Our study showed that the Fr-SF-SEAs (1:2) based on silk protein and silk short fibers exhibits great advantages in mechanical properties and hydrophilicity and can successfully optimize the inoculation of seed cells and regenerate ear-shaped cartilage tissue with high morphological fidelity by inoculating chondrocytes. Solving the problem of ear cartilage reconstruction in microtia patients is only one of the promising applications of this Fr-SF-SEAs (1:2), and as a scaffold with platform potential, there is every reason to believe that by loading with different cells, we can realize the need for diverse tissue regeneration and potentially solve other specific tissue-regeneration challenges in regenerative medicine. Despite some exciting results, it should be noted that the mechanical properties of the scaffolds rely mainly on short fibers, and their fiber length and more precise addition ratios need to be further optimized to achieve the best performance in terms of mechanical properties and morphological maintenance ability. Although there are still issues that require further experimental optimization, our results fully confirm the advantages and potential of Fr-SF-SEAs (1:2) scaffolds for tissue regeneration, providing a new platform and perspective for the construction of biological scaffolds and solid scientific evidence for future preclinical applications of tissue-engineered cartilage.

Conclusions

In conclusion, we developed a simple strategy using SF and silk fiber to fabricate diverse structural Fr-SF-SEAs (1:2) with physically and chemically crosslinked double network structures. Importantly, this approach is highly versatile and can be readily combined and applied to bioactive materials, such as physiologically active proteins and drugs, to build a biomimetic microenvironment for specific tissues. The Fr-SF-SEAs (1:2) displayed desirable synergistic properties, such as a honeycomb structure, hydrophilicity, elasticity and enhanced mechanical properties, for tissue engineering. These Fr-SF-SEAs (1:2) underwent cyclic compression inoculation to improve the efficiency and uniformity of cell

inoculation in vitro, and furthermore, their regenerated cartilage exhibited high morphological fidelity and tissue maturity in vivo. Moreover, the ear-shaped Fr-SF-SEAs (1:2) enabled stable and precise ear-bionic cartilage regeneration on a human scale, indicating that Fr-SF-SEAs (1:2) have clinical translational potential for microtia reconstruction.

Supplementary Information The online version contains supplementary material available at https://doi.org/10.1007/s42765-023-00266-8.

Acknowledgements We gratefully acknowledge financial support from the National Key Research and Development Program of China (2018YFC1105800, 2017YFC1103900), the National Natural Science Foundation of China (82102211, 81871502), the Shanghai Municipal Key Clinical Specialty (shslczdzk06601), the Shanghai Collaborative Innovation Program on Regenerative Medicine and Stem Cell Research (2019CXJQ01), the Key Research and Development Program of Henan Province (No. 221111310100), the Major Science and Technology Projects of Xinxiang City (No. 21ZD006), the Clinical Research Plan of SHDC (No. SHDC2020CR2045B), and the Start-up Funds of Talent Construction and Scientific Research in Shanghai 9th People's Hospital (2021rcyj-ld).

Data availability The data and materials are available.

Declarations

Conflicts of interest The authors declare no competing financial interests.

References

1. Lumelsky N, O'Hayre M, Chander P, Shum L, Somerman MJ. Autotherapies: enhancing endogenous healing and regeneration. *Trends Mol Med*. **2018**;*24*:919.
2. Wei W, Dai H. Articular cartilage and osteochondral tissue engineering techniques: recent advances and challenges. *Bioact Mater*. **2021**;*6*:4830.
3. Reid JA, Dwyer KD, Schmitt PR, Soepriatna AH, Coulombe KL, Callanan A. Architected fibrous scaffolds for engineering anisotropic tissues. **Biofabrication**. **2021**, ***13.***
4. Ju XJ, Liu XZ, Zhang Y, Chen X, Chen MM, Shen HS, Feng YH, Liu JS, Wang M, Shi Q. A photo-crosslinked proteinogenic hydrogel enabling self-recruitment of endogenous TGF-β1 for cartilage regeneration. *Smart Mater in Med*. **2022**;*3*:85.
5. Zhang YC, Gao HC, Luo HT, Chen DF, Zhou ZY, Cao XD. High strength HA-PEG/NAGA-Gelma double network hydrogel for annulus fibrosus rupture repair. *Smart Mater in Med*. **2022**;*3*:128.
6. Jia LT, Hua YJ, Zeng JS, Liu WS, Wang D, Zhou GD, Liu X, Jiang HY. Bioprinting and regeneration of auricular cartilage using a bioactive bioink based on microporous photocrosslinkable acellular cartilage matrix. *Bioact Mater*. **2022**;*16*:66.
7. Li Z, Gunn J, Chen MH, Cooper A, Zhang M. On-site alginate gelation for enhanced cell proliferation and uniform distribution in porous scaffolds. *J Biomed Mater Res A*. **2008**;*86*:552.
8. Radisic M, Euloth M, Yang L, Langer R, Freed LE, Vunjak-Novakovic G. High-density seeding of myocyte cells for cardiac tissue engineering. *Biotechnol Bioeng*. **2003**;*82*:403.
9. Miller JS, Stevens KR, Yang MT, Baker BM, Nguyen DH, Cohen DM, Toro E, Chen AA, Galie PA, Yu X, Chaturvedi R, Bhatia SN, Chen CS. Rapid casting of patterned vascular networks for perfusable engineered three-dimensional tissues. *Nat Mater*. **2012**;*11*:768.
10. Sari M, Hening P, Chotimah AID, Yusuf Y. Bioceramic hydroxyapatite-based scaffold with a porous structure using honeycomb as a natural polymeric Porogen for bone tissue engineering. *Biomater Res*. **2021**;*25*:2.
11. Buenzli PR, Lanaro M, Wong CS, McLaughlin MP, Allenby MC, Woodruff MA, Simpson MJ. Cell proliferation and migration explain pore bridging dynamics in 3D printed scaffolds of different pore size. *Acta Biomater*. **2020**;*114*:285.
12. Cengiz IF, Oliveira JM, Reis RL. Micro-CT—a digital 3D microstructural voyage into scaffolds: a systematic review of the reported methods and results. *Biomater Res*. **2018**;*22*:26.
13. Ci Z, Zhang Y, Wang Y, Wu GY, Hou MJ, Zhang PL, Jia LT, Bai BS, Cao YL, Liu Y, Zhou GD. 3D cartilage regeneration with certain shape and mechanical strength based on engineered cartilage gel and decalcified bone matrix. *Front Cell Dev Biol*. **2021**;*9*:638115.
14. Lee M, Bae K, Guillon P, Chang J, Arlov Ø, Zenobi-Wong M. Exploitation of cationic silica nanoparticles for bioprinting of large-scale constructs with high printing fidelity. *ACS Appl Mater Interfaces*. **2018**;*10*:37820.
15. Cengiz IF, Pereira H, Espregueira-Mendes J, Oliveira JM, Reis RL. Treatments of meniscus lesions of the knee: current concepts and future perspectives. *Regen Eng Transl Med*. **2017**;*3*:32.
16. Wang Y, Kim HJ, Vunjak-Novakovic G, Kaplan DL. Stem cell-based tissue engineering with silk biomaterials. *Biomaterials*. **2006**;*27*:6064.
17. Omenetto FG, Kaplan DL. New opportunities for an ancient material. *Science*. **2010**;*329*:528.
18. Wang Y, Rudym DD, Walsh A, Abrahamsen L, Kim HJ, Kim HS, Kirker-Head C, Kaplan DL. In vivo degradation of three-dimensional silk fibroin scaffolds. *Biomaterials*. **2008**;*29*:3415.
19. Zhao CX, Liu YW, Lv ZC, Cao LT, Ren J, Shao ZZ, Ling SJ. Silk Fibroin Nacre. *Adv Fiber Mater*. **2022**;*4*:1191.
20. Shao ZZ, Vollrath F. Surprising strength of silkworm silk. *Nature*. **2002**;*418*:741.
21. Rousseau ME, Lefèvre T, Beaulieu L, Asakura T, Pézolet M. Study of protein conformation and orientation in silkworm and spider silk fibers using Raman microspectroscopy. *Biomacromol*. **2004**;*5*:2247.
22. Zhang Y, Lu HJ, Liang XP, Zhang MC, Liang HR, Zhang YY. Silk materials for intelligent fibers and textiles: potential, progress and future perspective. *Acta Phys Chim Sin*. **2022**;*38*:2103034.
23. Lu HJ, Xia KL, Jian MQ, Liang XP, Yin Z, Zhang MC, Wang HM, Wang HM, Li S, Zhang YY. Mechanically reinforced silkworm silk fiber by hot stretching. *Research (Wash D C)*. **2022**;*2022*:9854063.
24. Zou SZ, Fan SN, Oliveira AL, Yao X, Zhang YP, Shao HL. 3D printed gelatin scaffold with improved shape fidelity and cytocompatibility by using antheraea pernyi silk fibroin nanofibers. *Adv Fiber Mater*. **2022**;*4*:758.
25. Lu HJ, Jian MQ, Yin Z, Xia KL, Shi SY, Zhang MC, Wang HM, Liang XP, Ma WG, Zhang X, Zhang YY. Silkworm silk fibers with multiple reinforced properties obtained through feeding Ag nanowires. *Adv Fiber Mater*. **2022**;*4*:547.
26. Wang Q, Ling SJ, Yao QZ, Li QY, Hu DB, Dai Q, Weitz DA, Kaplan DL, Buehler MJ, Zhang YY. Observations of 3 nm silk nanofibrils exfoliated from natural silkworm silk fibers. *ACS Mater Lett*. **2020**;*2*:153.
27. Zhang J, Allardyce BJ, Rajkhowa R, Zhao Y, Dilley RJ, Redmond SL, Wang X, Liu X. 3D printing of silk particle-reinforced chitosan hydrogel structures and their properties. *ACS Biomater Sci Eng*. **2018**;*4*:3036.
28. Huang L, Du XY, Fan SN, Yang GS, Shao HL, Li DJ, Cao CB, Zhu YF, Zhu MF, Zhang YP. Bacterial cellulose nanofibers

promote stress and fidelity of 3D-printed silk based hydrogel scaffold with hierarchical pores. *Carbohydr Polym*. **2019**;*221*:146.
29. Mandal BB, Grinberg A, Gil ES, Panilaitis B, Kaplan DL. High-strength silk protein scaffolds for bone repair. *Proc Natl Acad Sci USA*. **2012**;*109*:7699.
30. Jia LT, Zhang Y, Yao L, Zhang PL, Ci Z, Zhang W, Miao CL, Liang XQ, He AJ, Liu Y, Tang SJ, Zhang RH, Wang XY, Cao YL, Zhou GD. Regeneration of human-ear-shaped cartilage with acellular cartilage matrix-based biomimetic scaffolds. *Appl Mater Today*. **2020**;*20*: 100639.
31. Lei D, Yang Y, Liu ZH, Yang BQ, Gong WH, Chen S, Wang SF, Sun LJ, Song BY, Xuan HX, Mo XM, Sun BB, Li S, Yang Q, Huang SX, Chen SY, Ma YD, Liu WG, He CL, Zhu B, Jeffries EM, Qing FL, Ye XF, Zhao Q, You ZW. 3D printing of biomimetic vasculature for tissue regeneration. *Mater Horiz*. **2019**;*6*:1197.
32. Rodriguez A, Cao YL, Ibarra C, Pap S, Vacanti M, Eavey RD, Vacanti CA. Characteristics of cartilage engineered from human pediatric auricular cartilage. *Plast Reconstr Surg*. **1999**;*103*:1111.
33. Liu Y, Zhang L, Zhou GD, Li Q, Liu W, Yu ZY, Luo XS, Jiang T, Zhang WJ, Cao YL. In vitro engineering of human ear-shaped cartilage assisted with CAD/CAM technology. *Biomaterials*. **2010**;*31*:2176.
34. Zhou GD, Jiang HY, Yin ZQ, Liu Y, Zhang QG, Zhang C, Pan B, Zhou JY, Zhou X, Sun HY, Li D, He AJ, Zhang ZY, Zhang WJ, Liu W, Cao YL. In vitro regeneration of patient-specific ear-shaped cartilage and its first clinical application for auricular reconstruction. *EBioMedicine*. **2018**;*28*:287.
35. Li Q, Liu TY, Zhang L, Liu Y, Zhang WJ, Liu W, Cao YL, Zhou GD. The role of bFGF in down-regulating α-SMA expression of chondrogenically induced BMSCs and preventing the shrinkage of BMSC engineered cartilage. *Biomaterials*. **2011**;*32*:4773.
36. He AJ, Xia HT, Xiao KY, Wang TT, Liu Y, Xue JX, Li D, Tang SJ, Liu FJ, Wang XY, Zhang WJ, Liu W, Cao YL, Zhou GD. Cell yield, chondrogenic potential, and regenerated cartilage type of chondrocytes derived from ear, nasoseptal, and costal cartilage. *J Tissue Eng Regen Med*. **2018**;*12*:1123.
37. Li D, Yin ZQ, Liu Y, Feng SQ, Liu Y, Lu FJ, Xu Y, Min PR, Hou MJ, Li K, He AJ, Zhang WJ, Liu W, Zhang YX, Zhou GD, Cao YL. Regeneration of trachea graft with cartilage support, vascularization, and epithelization. *Acta Biomater*. **2019**;*89*:206.
38. Luo XS, Zhou GD, Liu W, Zhang WJ, Cen L, Cui L, Cao YL. In vitro precultivation alleviates post-implantation inflammation and enhances development of tissue-engineered tubular cartilage. *Biomed Mater*. **2009**;*4*: 025006.
39. Falsafi S, Koch RJ. Growth of tissue-engineered human nasoseptal cartilage in simulated microgravity. *Arch Otolaryngol Head Neck Surg*. **2000**;*126*:759.
40. Yin ZQ, Li D, Liu Y, Feng SQ, Yao L, Liang XQ, Miao CL, Xu Y, Hou MJ, Zhang RH, Zhang WJ, Liu W, Liu Y, Zhou GD, Cao YL. Regeneration of elastic cartilage with accurate human-ear shape based on PCL strengthened biodegradable scaffold and expanded microtia chondrocytes. *Appl Mater Today*. **2020**;*20*: 100724.
41. Visser J, Melchels FP, Jeon JE, van Bussel EM, Kimpton LS, Byrne HM, Dhert WJ, Dalton PD, Hutmacher DW, Malda J. Reinforcement of hydrogels using three-dimensionally printed microfibres. *Nat Commun*. **2015**;*6*:6933.
42. Mohabatpour F, Karkhaneh A, Sharifi AM. A hydrogel/fiber composite scaffold for chondrocyte encapsulation in cartilage tissue regeneration. *RSC Adv*. **2016**;*6*:83135.
43. Shen YB, Xu Y, Yi BC, Wang XL, Tang H, Chen C, Zhang YZ. Engineering a highly biomimetic chitosan-based cartilage scaffold by using short fibers and a cartilage-decellularized matrix. *Biomacromol*. **2021**;*22*:2284.
44. Muncie JM, Weaver VM. The physical and biochemical properties of the extracellular matrix regulate cell fate. *Curr Top Dev Biol*. **2018**;*130*:1.
45. Soans KG, Norden C. Shining a light on extracellular matrix dynamics in vivo. *Semin Cell Dev Biol*. **2021**;*120*:85.

Qianyi Wang entered Weifang Medical University in 2020 to pursue a master's degree. During his master's degree, he studies tissue engineering and focus on its clinical application with Prof. Guangdong Zhou. Currently, his current research involves biomaterials, tissue engineering for congenital facial deformities.

Xinyue Ran a master's student at the Institute of Plastic Surgery, Weifang Medical College, is currently engaged in cartilage tissue engineering-related research at Key Lab of Tissue Engineering, Shanghai Ninth People's Hospital. Her research interests lie in how to regulate stem cell chondrogenesis and maintain cartilage phenotype stability.

Jian Wang is a chief physician at Department of Plastic surgery, The Ninth People's Hospital Affiliated to Shanghai Jiao Tong University School of Medicine, China. He has been engaged in the clinical work of plastic and cosmetic surgery for many years and has accumulated rich clinical experience. He is proficient in all kinds of plastic and cosmetic surgeries and has unique insights into the management of the more difficult post-surgical complications in plastic surgery.

Sinan Wang entered Weifang Medical University in 2020 to pursue a master's degree. During his master's degree, He conducts his research mainly in Shanghai Key Lab of Tissue Engineering. He research interests lie in polymer materials science and cartilage regeneration technology.

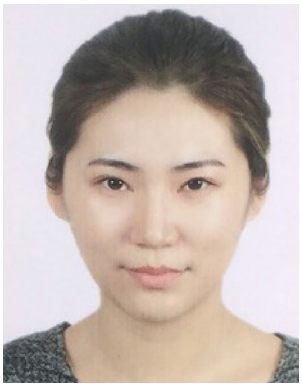

Peiling Zhang is a PhD candidate at Department of Plastic and Reconstructive Surgery, Shanghai Ninth People's Hospital. Her research interests lie in cartilage and bone regeneration technology.

Erji Gao is a PhD student at the Department of Thoracic Surgery, Shanghai Pulmonary Hospital, Tongji University School of Medicine. He received his MD from Shanghai Jiao Tong University School of Medicine in 2019. His current research involves cartilage regenerative biomaterials and tracheal reconstruction via tissue engineering.

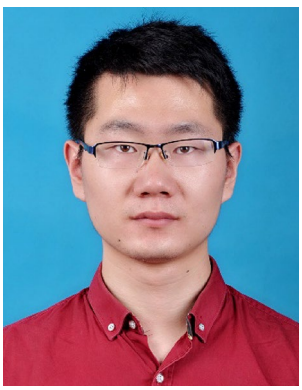

Baoshuai Bai is a PhD candidate in the Department of Orthopedics, Qilu Hospital of Shandong University. He used to do research in Shanghai Key Lab of Tissue Engineering. His research interests lie in the regeneration of cartilage, bone, and spinal cord.

Junfeng Zhang is doctoral supervisor of Shanghai Jiao Tong University School of Medicine. Member of Shanghai Medical Association Cardiovascular Branch and Science Branch, deputy chairman of Shanghai Society of Traditional Chinese Medicine Interventional Cardiology Branch. In recent years, he has focused on the field of thrombosis and antithrombotic research, as well as the transformation of implant devices.

Guangdong Zhou is a Professor of Medical College of Shanghai Jiaotong University, Executive Vice-Director of National Center for Tissue Engineering Research, Former Secretary-General and Executive Director of Tissue Engineering and Regenerative Medicine Branch of Chinese Society of Biomedical Engineering. He has long been engaged in functional cartilage regeneration and clinical application transformation, construction of cartilage in vitro and precise regulation of its three-dimensional morphology (auricle, trachea, etc.), and repair of various cartilage defects in large animals.

Dong Lei received his Ph.D degree in 2020 from Donghua University (With Prof. Zhengwei You). Then after worked as a research and development personnel at Shanghai Haohai Biological Technology Co. Ltd. In 2021, he joined Shanghai Key Lab of Tissue Engineering at Shanghai 9th People's Hospital and Shanghai Jiao Tong University School of Medicine as a research associate. His current research focuses on biomaterials, 3D printing and biomimetic scaffolds for cardiovascular treatment and cartilage regeneration.